Accretion Disks and Stellar Jets Around T Tauri Stars

François MÉNARD[1], Catherine DOUGADOS, Claudia LAVALLEY
Laboratoire d'Astrophysique, Observatoire de Grenoble, CNRS-UJF
BP 53, F-38041 Grenoble cedex 9, France (menard@cfht.hawaii.edu)

Sylvie CABRIT
DEMIRM, Observatoire de Paris, 61 Ave. de l'Observatoire, 75014 Paris, France

and

Karl STAPELFELDT
MS 183-900, Jet Propulsion Laboratory, 4800 Oak Grove Drive, Pasadena, CA 91109, USA

Abstract. Results from Adaptive Optics imaging of accretion disks and stellar jets around pre-main sequence T Tauri stars are presented. The data were obtained with PUEO, the Adaptive Optics Bonnette attached to the Canada-France-Hawaii Telescope (CFHT). The results on mass loss include a study of the morphology of the jet in the multiple star RW Aur. Also, a study of the morphology and proper motions of emission knots in the micro-jet of DG Tau is presented. On the other hand, the results on mass accretion include images and models in the optical and near infrared of the scattered light by the accretion disk surrounding HK Tau B. The optical images are from WFPC2, on board HST. Many geometrical parameters of the disk are deduced (e.g., inclination, radius). So are the vertical scale height and the surface density distribution of the grains responsible for the scattered light. The disk mass is also estimated. This exemple shows how the Hubble Space Telescope and ground-based adaptive optics imaging can be use to complete each other.

1. Introduction

Theoretical and observational investigations of the stellar formation process relevant for low mass stars results naturally in the formation of a circumstellar disk. This disk may then evolve into a planetary system. The current accepted scenario of star formation includes an embedded phase with a so-called Class I infrared spectral energy distribution (SED) which rises longward of 2 μm. The excess infrared energy emitted comes in part from thermal re-emission of the starlight absorbeb in the circumstellar envelope and in part from thermal emission in the disk. A Classical T Tauri phase (CTTS, or Class II) follows during which the massive envelope disperses but accretion continues through the optically thick disk. Only the infrared excess from the disk remains. Finally, the objects "evolve" to the Weak-line T Tauri stage (WTTS, or Class III), when accretion through the now optically thin disk subsides due to lack of replenishment (leading to the rapid dissipation of the disk) and/or gaps opened by planet formation. No near- and mid-infrared excess is left at that stage.

Also associated to the star formation process is an episode mass loss, often bipolar and orthogonal to the disk plane. This outflow activity can take many faces at all stages of the evolution. Low velocity molecular outflows and high velocity ionized atomic jets, often associated with arc-shaped Herbig-Haro objects (i.e., the bow shocks of the jets) are detected. The latter being found on scales ranging from $0\farcs1$ to $1000''$, i.e., from 15 AU to 1pc from the star for an object located at a distance of about 150pc, that of the nearest star forming regions.

Studying accretion and ejection is important because increasing our knowledge of these phenomena individually will ultimately lead to a better understanding of the pivotal, but yet unidentified, connection between them. For example, although it is accretion in the first place that allows the star to grow to its final mass, the mass loss controls, at least in part, the angular momentum evolution of the star. Therefore, it regulates the final stellar mass too. The accretion disk, in turns, providing the power to drive the ejection. High angular resolution and spectral resolution as low as a few thousands would allow us to study the acceleration and collimation process at scales of 15 to 100AU.

[1]On leave at the Canada-France-Hawaii Telescope Corporation, P.O. Box 1597, Kamuela, HI 96743, USA.

The mass loss phenomenon spans many orders of magnitude in time. It occurs in objects as young as 10^4 years old and as old as a few 10^6 years old. It seems however that the mass loss rate decreases with time in general.

During the Class I phase, mass loss is intense. However, the driving source is often totally embedded, being invisible at optical and infrared wavelengths. The highly collimated optical jets and the associated chains of Herbig-Haro objects trace the outward motion of the material ejected from the star/disk system out to distances as large as a few parsecs. See, e.g., Bachiller (1996) and Bally et al. (1996) for reviews.

During the class II phase, the Classical T Tauri phase, the outflow manifestations are more modest. The signatures of mass loss are found in low-excitation atomic forbidden lines. They extend over distances of a few arcsecs, corresponding to a few hundreds of AU's at the distance of the closest star forming regions. They are called micro-jets. The fact that the line profiles are almost systematically blue-shifted was also long considered as a good, although indirect, evidence that opaque (accretion) disks existed.

The Classical T Tauri stars are therefore ideal laboratories to study the accretion and ejection processes. They still have opaque accreting disks that can be imaged. The mass accretion rates are well determined. They also drive optical jets tracing the mass-loss, but these jets are small. They are relatively evolved so that their original envelope has dissipated for the most part. As a consequence, the extinction is low and we can hope to directly see details close to the centre, where the jet is thought to be launched from. The choice to select Classical T Tauri stars as targets for adaptive optics imaging is therefore a compromise between the detectability of the features close to the objects and the surface brightness of these features.

In the following sections we will describe recent results on the physical properties of accretion disks (§2) and on the morphology and kinematics of stellar micro-jets (§3). Some of the figures are presented here for the first time.

2. Physical Properties of Accretion Disks

As we briefly discussed above, the accretion and ejection processes are driven by a yet unknown mechanism(s) but they appear to be thightly linked together as was demonstrated by Cabrit et al. (1990) and Hartigan et al. (1995). This is true from the very early stages of stellar formation, the so-called Class O phase, until the later Classical T Tauri star phase (Class II). Because the equatorial disk is (likely) instrumental in both processes, either as a reservoir of material or as an energy source, obtaining a better knowledge of the detailed structure of accretion disks is fundamental to better constrain the accretion/ejection models now available in the literature.

Models and numerical simulations show that the near-infrared ($\lambda < 10\mu$m) *thermal* emission of an accretion disk occurs in the innermost 0.1AU. To observe that zone directly, very high dynamic range is needed as well as very high angular resolution (Malbet & Bertout, 1995). This should be reached by the VLTI (Ménard et al. 1997). A first detection proving the feasibility, and at the same time confirming the model for FU Orionis stars, was achieved lately by Malbet et al. (1998) who resolved the 2.2μm *thermal* emission of the accretion disk around FU Orionis by long-base (100m) interferometry using the Palomar Testbed Interferometer.

The outcome of these observations is not an image however. It is a visibility, a single point of measurement in the Fourier plane, the *uv*-plane. Although this is already a great result, near-infrared long-baseline interferometry will not yield detailed images of disks before the next decade when multi-baseline observations become available. Other high resolution imaging techniques are becoming available however, and much may still be learned regarding the fine structure of the accretion disks before aperture synthesis imaging in the optical and near infrared becomes available.

For example, observation of the *scattered* starlight from the surface of accretion disks offers a different way to extract information and to study disks. Since the commissioning of performant high resolution imagers, including the *Hubble Space Telescope* but also *ground-based adaptive optics systems*, examples of disk detections have been numerous in the literature.

The first results, when compared with millimeter interferometry of the gaseous component of the disk, mostly CO, rapidly showed that AO is powerful and reliable to evaluate some of the disk parameters (e.g., Roddier et al. (1996), and Dutrey, Guilloteau and Simon (1994) for GG Tau; Duvert et al. (1998) and Close et al. (1998) for UY Aur).

In the following we will discuss the recent discovery of another disk, around the classical T Tauri star HK Tau B. This objects was imaged quasi-simultaneously with HST/WFPC2 in the optical and with CFHT/PUEO in the near-infrared. The results are presented in Figure 1. They show the complementarity between space-born direct imaging and ground-based adaptive optics observations.

These results are interesting because they are the first images of a *circumstellar* disk around one component of a binary system. From the images in Fig.1 we can directly extract a few geometrical parameters of the disk. The disk has a very similar extent at all wavelengths, $\sim 1\farcs5$ or 210AU in diameter. This tells us that the edges are likely to be fairly sharp.

Also, this is the smallest disk resolved so far. Because the projected separation of the two components is only 3 times

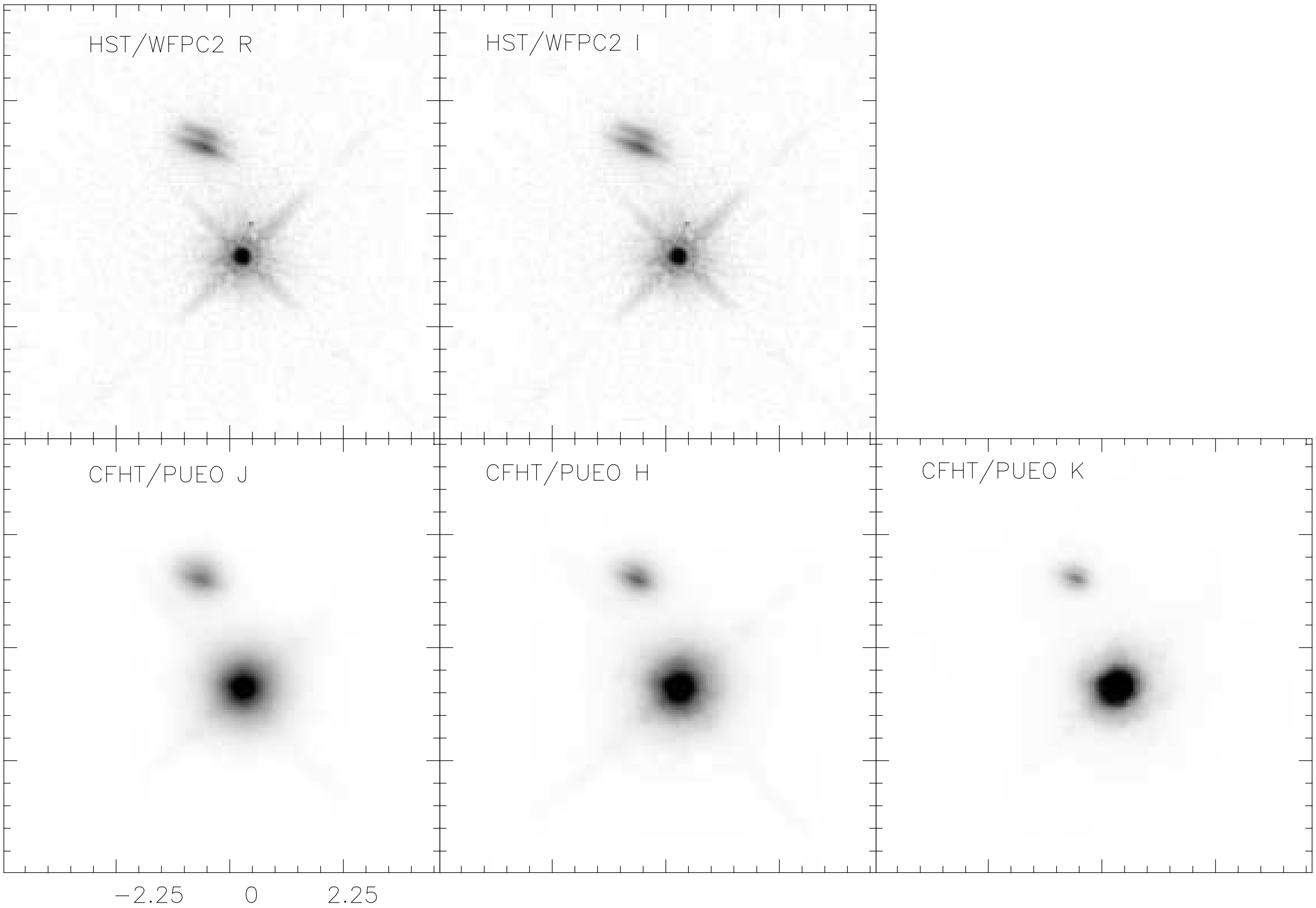

Figure 1: Images of the pre-main sequence binary star HK Tau. The separation between the two stars is $2\farcs4$. The optical images were obtained with WFPC2 onboard HST. The near-infrared images were obtained at the Canada-France-Hawaii Telescope with the PUEO adaptive optics bonnette and the KIR camera.

larger than the disk radius, it is interesting to ask whether there is a causal link between the small size of the disk and the presence of a companion! It is too early to conclude, but systems like HK Tau contain the answer to that question.

The disk further appears quasi edge-on, with the north-west nebula slightly brighter than the south-east one. Numerical simulations of the scattered light by the disk gives $i = 5^o \pm 1^o$. The central star is not seen either, even at 2.2μm where the extinction is 10 times smaller than in the visual. Given our detection limit, we estimate that $\mathrm{A_v} > 50$ magnitudes of extinction in the plane of the disk.

The nearly edge-on orientation is very favorable to study the scale height of the dust distribution in the disk plane. That possiblity was discussed and tested extensively by Burrows et al. (1996) in the case of HH 30. For HK Tau, numerical simulations of the scattered starlight also allows to evaluate many of the disk physical parameters, see Stapelfeldt et al. (1998) for more details.

The results presented in Fig. 2 were obtained for single scattering of the starlight by spherical dust grains (Mie scattering) distributed in the disk with a parametrized surface density $\Sigma(r) = \Sigma_0(r/r_0)^p$ and Gaussian vertical density profile $\rho(z) = \rho_0 \exp[-z^2/H(r)^2]$. This vertical profile is valid for vertically isothermal, hydrostatic, non-self-gravitating disks. A parametrized scale height $H(r) = H_0(r/r_0)^\beta$ was further assumed. Following the numbers extracted from Fig.1, we adopted an outer radius of 105 AU. A χ^2 minimization procedure was used to solve for the disk parameters. Stapelfeldt et al. (1998) present a discussion of the results from various models and discuss the reliability of the solution presented here.

The normalization H_0 of the scale height is 3.8AU at $r = 50$AU. This number is well constrained. The disk of HK Tau B is significantly flatter than that of HH30. For HH30, $H_0 = 15.5$AU at $r = 100$AU. Presented differently, at 50AU the ratio

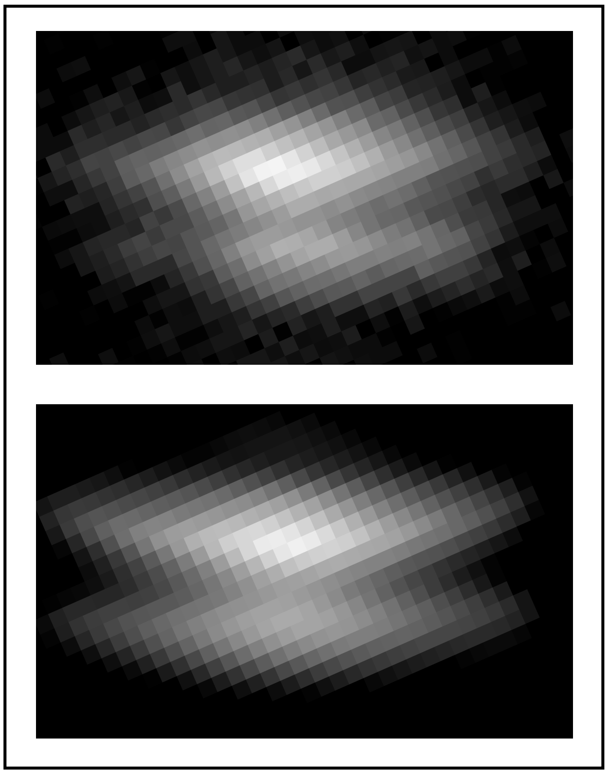

Figure 2: Best-fit model of the scattered light compared to the F814W-image from HST. The image is from Stapelfeldt et al. (1998). The top panel shows the observations, the bottom panel the best fit model from single scattering numerical simulations. The field of view is $1\overset{''}{.}6 \times 1\overset{''}{.}0$.

$H/r = 0.08$ for HK Tau but 0.12 for HH30. The disk mass of an edge-on disk is directly related to the "thickness" of the dark lane (See Burrows et al. 1996). For HK Tau, we estimate a total disk mass of $\sim 6 \times 10^{-5}$ $M_\odot$ in dust and gas, if the grains have interstellar properties. This is small with respect to the minimum mass solar nebula. It is also small with respect to the mass implied by the 1.3mm continuum flux density (40 mJy) detected by Osterloh & Beckwith (1995). The expected disk mass from this mm-flux is roughly 100 times larger. Possible explanations are that (1) the mm-flux is associated to the primary whose disk remains undected so far by direct imaging because oriented at a less favorable inclination, or (ii) a fraction of the grains in HK Tau B's disk are large, and therefore do not scatter light efficiently, leading us to grossly underestimate the disk mass from scattered light models alone.

Figure 3 shows models of the scattered light by the disk. The right panel (K-band) shows that the central star remains undetected in the near infrared, i.e., the disk remains optically thick. These observations and models show clearly that even a very low mass of dust and gas is enough to produce an optically thick disk, to totally block the direct starlight, and to make the "silhouette" of the disk detectable given the inclination is favorable.

Optical and near-infrared images of the *scattered light* of disk seen nearly edge-on are therefore very sensitive tools to examine the circumstellar environment of pre-main sequence objects. Such low mass disks would probably not be detected if seen more pole-on, but they would remain at the detection limit of the current millimeter interferometers. Both techniques complete each other nicely.

On the other hand, observations on the larger 8-m class telescopes should also provide us with yet another gain in angular resolution, typically of a factor of 4 for the surface of the PSF, but also a gain in contrast due to the larger collective area. There is no doubt that numerous fainter disks will be imaged in the near future.

3. Structure and Kinematics of Stellar Jets

Outflow phenomena are believed to play an important role in the regulation of the star formation process. In particular, the final mass of a star is dictated by an intricate interplay between accretion of material from the circumstellar envelope and equatorial disk and mass-loss, in the form of ionized atomic jets and molecular outflows. While the existence of a link between ejection and accretion is now well established (Cabrit et al. 1990; Hartigan et al 1995), the detailed physical process involved is still poorly constrained. MHD models (Ferreira & Pelletier 1993, 1995; Shu et al. 1995), where the magnetic field extracts

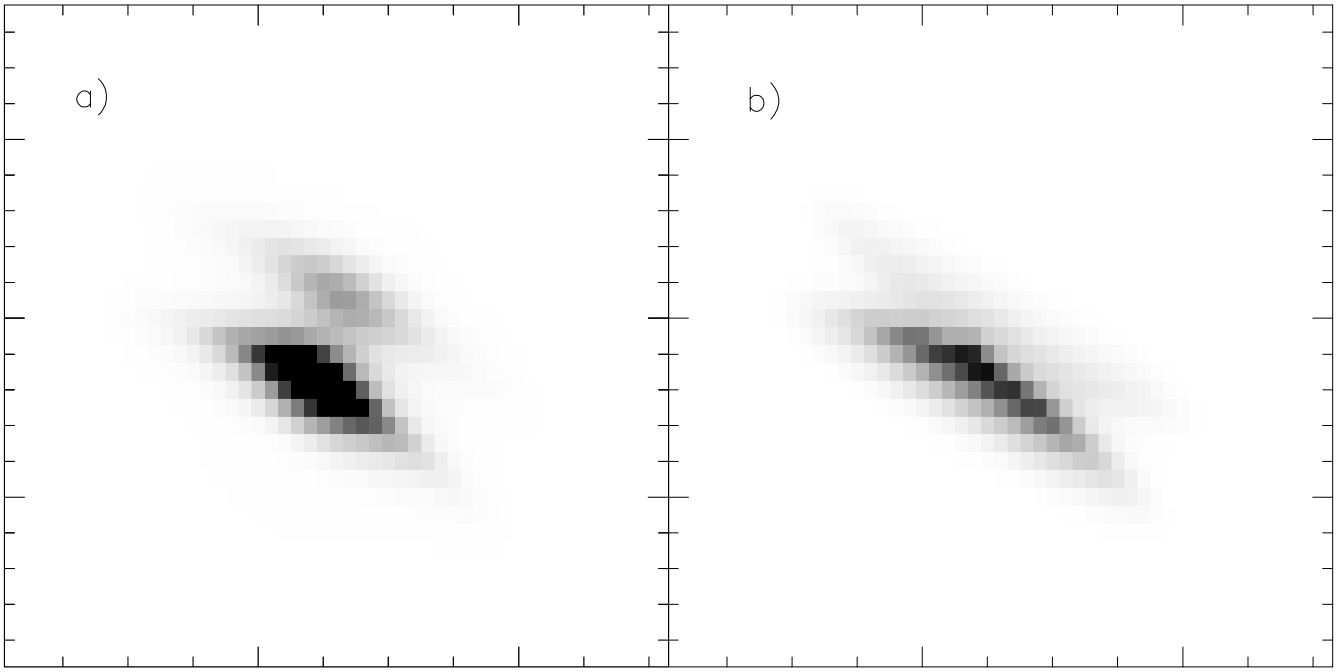

Figure 3: **a)** I-band scattered light model image of HK Tau, **b)** K-band scattered light model image of HK Tau. The dark lane is narrower at K-band.

angular momentum from the accreting disk, provide to date the most coherent physical description. These models predict that most of the collimation and acceleration processes occur over distances less than 100 AU. Constraining the geometry and the excitation conditions in the wind at such scales is thus essential to our understanding of the mass loss process in young stars.

The optically revealed classical T Tauri stars offer an unique opportunity to answer these questions. Indeed, although outflow manifestation is most spectacular around the youngest embedded sources (age $<$ a few 10^5 yrs), where collimated jets extending over a few parsecs are detected, the presence of substantial circumstellar environment at these stages prevents the study of the innermost regions of the wind. Classical T Tauri stars (CTTs) are typically an order of magnitude older (age $\simeq 10^6$ yr) and have accreted/dissipated most of their original envelope. The photosphere is therefore directly detectable, but they still possess an optically thick, accreting equatorial disk and spectral signatures indicating ongoing mass-loss. In particular, the blueshifted optically thin emission of weakly ionized atoms (such as [O I], [S II], [N II]) present in their optical spectra allow to trace outflowing material within a few 100 AU's of the central source. The detailed study of these forbidden line emission regions (FLERs) is however impaired by the proximity of the strong stellar continuum.

The long-slit spectroscopic observations of Solf and collaborators, by allowing accurate subtraction of the continuum emission, provided the first direct evidence for jet-like forbidden line emission extending over a few arcseconds around a dozen or so T Tauri stars (Hirth et al. 1997). Terminal velocities of 100-200 km/s are reached over typically a few arcsec. These observations also showed the existence of complex velocity and excitation gradients along the jet. Without full 2-D information however, no firm conclusion could be reached on the excitation and collimation processes.

Significant advance on this subject became recently possible with the availability of adaptive optics system in the optical regime, allowing to reach spatial resolutions of $\simeq 0.2''$. We report here on the first narrow band images in the [S II]6731,6716 Å and [O I]6300 Å lines of the small scale jets associated with 2 CTTs: DG Tau and RW Aur. These observations allow a detailed morphological study of the mass-loss in these stars.

3.1. Morphology of the Jets

We first illustrate some of the general morphological aspects of the 2 jets on one specific case: the binary Classical T Tauri star RW Aurigae. Figure 4 presents the low-excitation [S II] image derived from narrow-band adaptive optics imaging.

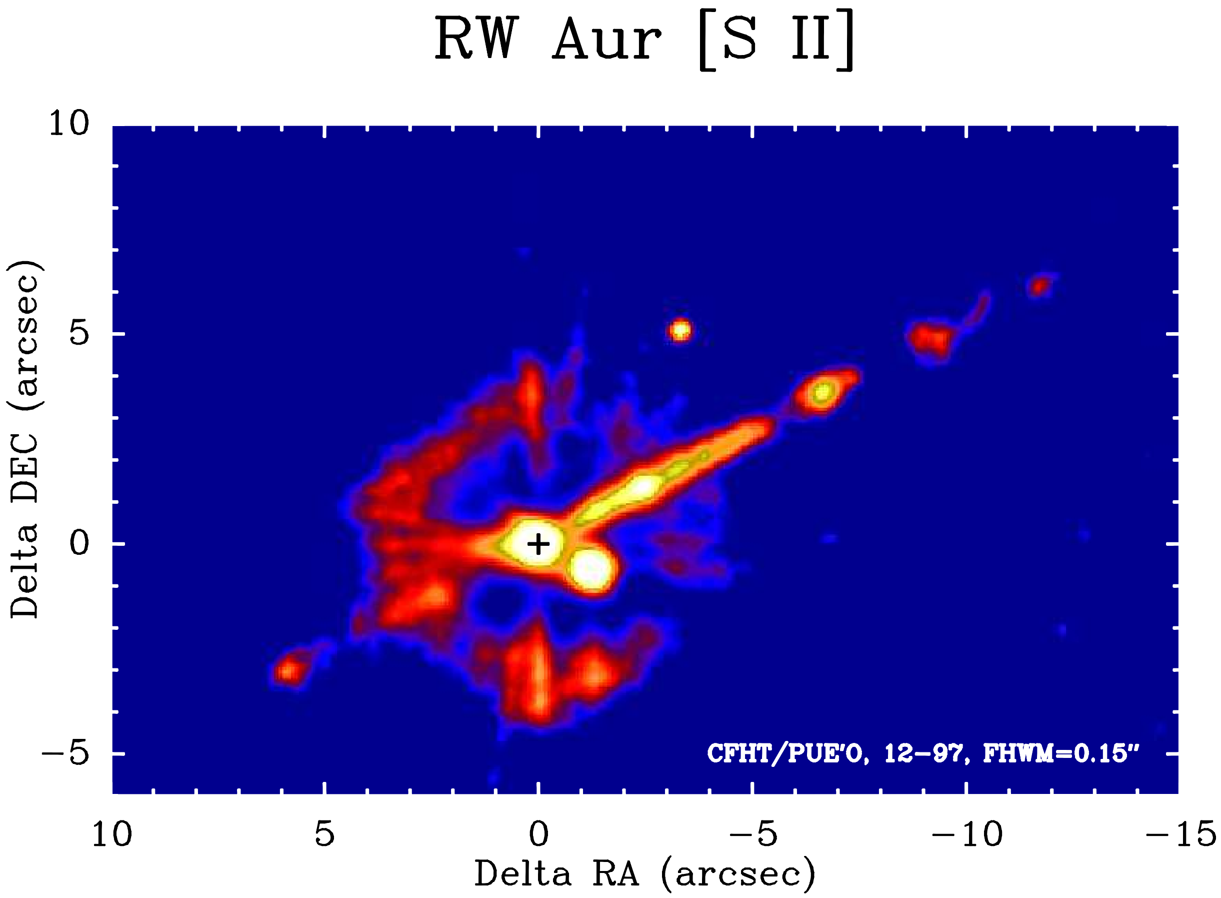

Figure 4: Optical image of the pre-main sequence binary RW Aur obtained at CFHT with PUEO. The micro-jet around RW Aur A is clearly visible in this [SII]$\lambda\lambda$6717/6731Å+ continuum deconvolved map. The resolution (FWHM) is $0.''15$. This image is the combination of three core-saturated exposures (300sec each) with two unsaturated images. The final dynamic range is $\sim 10^5(3\sigma)$. The centroid position of RW Aur A is indicated by a black cross.

Forbidden line emission nicely traces the jet out to $10''$. RW Aur-A, the primary component of the system, is clearly identified as the source of the wind. The emission, both in [S II] and [O I], is dominated by knots separated by typically a few arcseconds. This morphological feature is very reminiscent of what is observed in the younger HH jets. The two jets are resolved transversally down to $\simeq 0.5''$ from the central star with radii ranging from 30-40 AU (RW Aur) to 100 AU (DG Tau). These values are again quite comparable to what has been derived from HST observations for the inner regions of HH jets (Ray et al. 1996). In both cases, either the wind originates from a large range of radii in the disk or the collimation must take place on scales less than 70 AU.

In addition, the RW Aur case brings some insight on the accretion/ ejection process in binary systems. This is the first time that such a jet is resolved in a close young binary system. This result is important because tidal torques are expected to disrupt or modify (warp) the structure of accretion disk in close binaries. The jet associated to RW Aur-A appears remarkably straight and morphologically similar to ionised jets detected around single stars. Assuming the disk is instrumental in launching the jet, this result means that any modification in the disk is not important enough to alter the jet propulsion mechanism. This could be because the jet is launched from the central part of the disk, a zone that remains unperturbed by the companion star because it is located deep enough in the potential well of the star it is orbiting. Indirect support for this picture comes from mm-flux measurements that are lower on average for binaries than for singles (Dutrey et al. 1996, Osterloh & Beckwith 1995) and from near- and mid-infrared excess that are comparable (Prato and Simon 1997). This is interpreted as evidence that

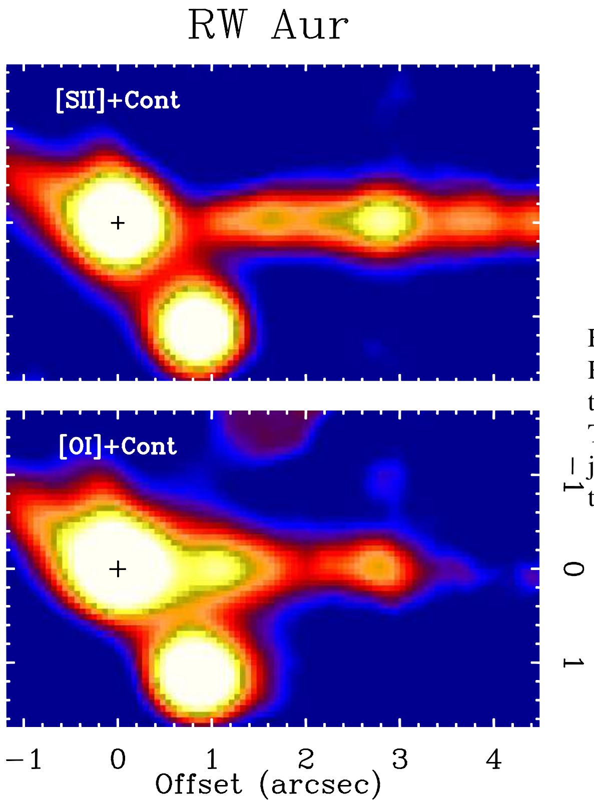

Figure 5: Comparison of the microjet structure of RW Aur A as traced by the [SII] and [OI] lines. The two frames have the same spatial resolution (0.15″). The [OI] emission decreases very rapidly along the jet. Note the location of the first [OI] knot (at 0.″9) that has no counterpart in the [SII] image.

the outer, colder parts of the circumstellar disks have been removed by (tidal) interactions, the inner, hotter part remaining unchanged.

3.2. Physical Parameters in the Jets

A detailed analysis of the physical parameters within the jet is also possible by studying various tracers, sensitive to different temperature and electron density conditions. Figure 5 presents a comparison of two images obtained in the [S II] and [O I] lines for the RW Aur jet. Clear excitation gradients are present along the jet. The body of the jet is brighter and better defined in the low-excitation [SII] line. The brigth emission knot, located 3″ away from RW Aur-A, is brighter in [SII] than [OI]. However, close to the source, a bright knot is visible in the [OI] line but undetected in [SII]. Generally, the [O I]/[S II] ratio increases towards the star, consistent with an augmentation of the electron density. A more detailed study of the excitation conditions in the jets will be presented elsewhere (Dougados et al. 1998).

The commissionning of integral field spectrographs like *GraF* and *OASIS* behind adaptive optics systems is very exciting and will bring better evaluations of the physical conditions and excitation mechanisms in stellar jets. The results obtained (without adaptive optics) and presented by Lavalley et al. (1996) give a good overview of the power of the method and of what will be achieved in the near future.

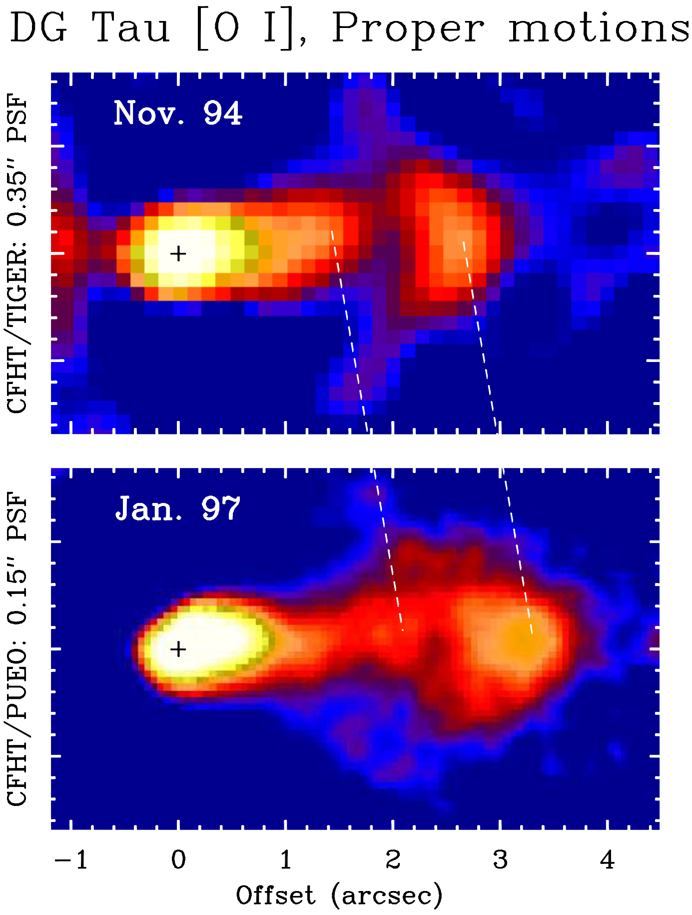

Figure 6: Proper motions in the jet of DG Tau. The upper panel shows, in log scale, the [OI]λ6300Å continuum subtracted map obtained with a spectro-imager at CFHT (TIGER) in November 1994 (See Lavalley et al. 1997). The lower panel shows, at the same spatial scale, the deconvolved [OI]λ6300Å + continuum map obtained at CFHT with PUEO in January 1997 (spatial resolution 0.15″). The displacement of the bow-shaped knot between these two epochs is $0\farcs5$, corresponding to a proper motion of $0\farcs2 \mathrm{yr}^{-1}$ and a tangential velocity of 150km/sec.

3.3. Excitation Conditions in the Jets

Constraints on the excitation conditions in the jets are derived from a detailed study of DG Tau. We show in Figure 6 two [O I] maps of this jet derived from 1) spectro-imaging observations at 0.4″ spatial resolution performed in November 1994 and 2) narrow-band adaptive optics imaging with 0.15″ resolution obtained in January 1997. In both images, the outer knot located at 3″ from the central source is clearly bow-shaped. In addition, the high angular resolution allows precise astrometry to be performed, relative to the position of the driving source. As indicated in Figure 6, the bow-shaped knot is clearly not a stationary feature in the jet. Its measured proper motion amounts to $0\farcs2 \mathrm{yr}^{-1}$, corresponding to a tangential velocity of 150 km/s. This, combined with previously measured transverse velocity gradients, suggest an internal working surface nature for this knot. Such internal shocks could arise from variability in the ejection velocity as already proposed for HH objects by Raga and collaborators (e.g., Raga et al 1990).

Note that the DG Tau jet looks far more perturbed than the RW Aur one with apparent wiggles that may suggest precession and/or strong interaction with the ambient medium. The jet width is also typically twice the one of the RW Aur jets.

The availability of adaptive optics techniques in the optical domain thus led to significant recent advances on the study of mass-loss from young stars. First direct detection of the jets associated with 2 CTTs could be achieved leading to new constraints on ejection and collimation mechanisms: 1) the morphology of these jets is very similar to the one of their younger HH jets counterpart suggesting a common physical origin and possible evolutionary scenario, 2) time variability on timescales of 5-10 yr plays an important role, 3) collimation processes occur on scales less than 70 AU.

To derive meaningful conclusions on the mass-loss process however, the study of a larger sample of sources is mandatory. As discussed above, spectacular progress in this field is expected soon from the combination of adaptive optics with spectro-imaging techniques, which will allow to: 1) probe the very inner parts ($< 0\farcs5$) of the jets, which hold key constraints on the collimation process, by providing accurate subtraction of the continuum; 2) study the kinematics with velocity resolution $\simeq$ 100 km/s and spatial resolution of 20 AU, allowing to probe directly the acceleration zone; 3) reliably constrain the excitation conditions close to the source through flux calibrated line intensities. Predictions from MHD models will thus be soon directly confronted with observations.

Acknowledgements

We are grateful to many colleagues at the Laboratoire d'Astrophysique de l'Observatoire de Grenoble. Thanks go to Jérôme Bouvier for his help and collaboration during the acquisition and analysis of the HK Tau data. Thanks also to Gilles Duvert, Fabien Malbet, and Gaspard Duchêne for many fruitful discussions.

References

Bachiller, R. 1996, ARA&A, 34, 111
Bally, J., Morse, J., Reipurth, B. 1996, *Science with the Hubble Space Telescope II*, (STScI, Baltimore), p.491
Burrows, C.J., Stapelfeldt, K.R., Watson, A.M., et al. 1996, ApJ, 473, 437.
Cabrit, S., Edwards, S., Strom, S.E., Strom, K.M., 1990, ApJ, 354, 687.
Close, L.M., Dutrey, A., Roddier, F., et al. 1998, ApJ, 499, 883.
Dougados, C., Lavalley, C., Cabrit, S., Ménard, F. 1998, A&A, in prep.
Dutrey, A., Guilloteau, S., Simon, M. 1994, A&A, 286, 149.
Dutrey, A., Guilloteau, S., Duvert, G., Prato, L., Simon, M., Schuster, K., Ménard, F. 1996, A&A, 309, 493.
Duvert, G., Dutrey, A., Guilloteau, S., et al. 1998, A&A, 332, 867.
Ferreira, J., Pelletier, G. 1993, A&A, 276, 625.
Ferreira, J., Pelletier, G. 1995, A&A, 295, 807.
Hartigan, P., Edwards, S., Gandhour, L., 1995, ApJ, 452, 736
Hirth, G.A., Mundt, R., Solf, J., 1997, A&AS, 126, 437
Lavalley, C., Cabrit, S., Dougados, C., Ferruit, P., Bacon, R. 1997, A&A, 327, 671.
Malbet, F., Berger, J.-P., Colavita, M.M., et al. 1998, ApJ, 507, L149.
Malbet, F., Bertout, C. 1995, A&AS, 113, 369.
Ménard, F., Malbet, F., Monin, J.-L., et al. 1997, in Proc. of the ESO workshop:*Science with the VLT Interferometer*, ed. F. Paresce, (Springer:Heidelberg), p. 248.
Osterloh, M., Beckwith, S.V.W. 1995, ApJ, 439, 288.
Prato, L., Simon, M., 1997, ApJ, 474, 455
Raga, A.C., Canto, J., Binette, L., Calvet, N., 1990, ApJ, 364, 601
Ray, T.P., Mundt, R., Dyson, J.E., Falle, S.A.E.G., Raga, A.C., 1996, ApJ, 468, L103
Roddier, C., Roddier, F., Northcott, M.J., Graves, J.E., Jim, K. 1996, ApJ, 463, 326.
Shu, F.H., Najita, J., Ostriker, E.C., Shang, H., 1995, ApJ, 455, L155
Stapelfeldt, K.R., Krist, J.E., Ménard, F., Bouvier, J., Padgett, D.L., Burrows, C.J 1998, ApJ, 502, L65.